Characterization of the Heparin/Heparan Sulfate Binding Site of the Natural Cytotoxicity Receptor NKp46†

Alon Zilka,[‡,§] Guy Landau,[‡,§] Oren Hershkovitz,[§] Noga Bloushtain,[§] Ahuva Bar-Ilan,[§] Fabrice Benchetrit,[§] Eyal Fima,[§] Toin H. van Kuppevelt,[||] John T. Gallagher,[⊥] Sharona Elgavish,[#] and Angel Porgador*[,§]

Department of Microbiology and Immunology, Faculty of Health Sciences, and Cancer Research Center, Ben Gurion University of the Negev, Beer Sheva 84105, Israel, Department of Biochemistry, University Medical Center, NCMLS, Nijmegen, The Netherlands, Department of Medical Oncology, University of Manchester, Cancer Research UK, Christie, Hospital NHS Trust, Manchester M204BX, United Kingdom, and The Bioinformatics Unit, The Hebrew University−Hadassah Medical School, Jerusalem 91120, Israel

Received June 28, 2005; Revised Manuscript Received September 4, 2005

ABSTRACT: NKp46 is a member of a group of receptors collectively termed natural cytotoxicity receptors (NCRs) that are expressed by natural killer (NK) cells. NCRs are capable of mediating direct killing of tumor and virus-infected cells by NK cells. We have recently shown that NKp46 recognizes the heparan sulfate moieties of membranal heparan sulfate proteoglycans (HSPGs), thus enabling lysis of tumor cells by NK cells. In the current study, we further examined the residues in NKp46 that may be involved in heparan sulfate binding on tumor cells. On the basis of both the electrostatic potential map and comparison to the heparin binding site on human fibronectin, we predicted a continuous region containing the basic amino acids K133, R136, H139, R142, and K146 to be involved in NKp46 binding to heparan sulfate. Mutating these amino acids on NKp46D2 to noncharged amino acids retained its virus binding capacity but reduced its binding to tumor cells with a 10−100 fold lower K_D when tested for direct binding to heparin. The minimal length of the heparin/heparan sulfate epitope recognized by NKp46 was eight saccharides as predicted from the structure and proven by testing heparin oligomers. Testing selectively monodesulfated heparin oligomers emphasized the specific contributions of O-sulfation, N-sulfation, and N-acetylation to epitope recognition by NKp46. The characterization of heparan sulfate binding region in NKp46 offers further insight into the identity of the ligands for NKp46 and the interaction of NK and cancers.

Natural killer (NK)[1] cells are a major component of the cellular mechanisms by which an immune response leads to the destruction of transformed or virus-infected target cells (*1*, *2*). The interaction between NK cells and their targets is mediated via various NK receptors and ligands (*3*−*5*). Heavily implicated in this interplay are inhibitory receptors of the NK cell surface, with classical and nonclassical MHC class I molecules as their ligands. With regard to activation receptors, three lysis receptors, expressed mainly on human NK cells, were recently identified. These natural cytotoxicity receptors (NCRs) include the NKp30, NKp44, and NKp46 molecules, all of which are capable of mediating direct killing of tumor and virus-infected cells. These NCRs are specifically expressed on NK cells; NKp30 and NKp46 precisely mark NK cells, whether resting or activated, while NKp44 is expressed by activated NK cells only (*3*, *5*). The NCRs are specific for non-MHC ligands (*3*, *5*); the nature of these ligands, cancer-expressed or virus-induced, is undefined with three exceptions: (i) NKp46 and NKp44, but not NKp30, bind to the hemagglutinin of influenza virus and the hemagglutinin neuraminidase of sendai virus (*6*−*9*); (ii) NKp30 interacts with pp65, the main tegument protein of human cytomegalovirus (*10*); and (iii) we recently observed that membrane-associated heparan sulfate is involved in the recognition of cellular ligands by NKp30 and NKp46 (*11*, *12*). The presence of the viral hemagglutinins on the virus-infected cells and the membranal heparan sulfate on the tumor cells is required for lysis of the corresponding virus-infected and transformed target cells by NK (*6*−*9*, *11*, *12*).

We previously showed that the membrane-proximal domain (NKp46D2), but not membrane-distal domain (NKp46D1), of NKp46 retained the binding of NKp46 to tumor cells (*7*). Target cell surface heparan sulfate proteoglycans (HSPGs) are recognized by NKp46D2. In ac-

† This study was supported by grants from the Prostate Cancer Foundation Israel, the Cancer Research Institute (CRI), and the Israel Cancer Research Foundation (ICRF). This work was also supported by the Cooperation Program in Cancer Research of the Deutsches Krebsforschungszentrum (DKFZ) and Israel's Ministry of Science (MOS).

* To whom correspondence should be addressed. Telephone: (972)-86477283. Fax: (972)-86477626. E-mail: angel@bgu.ac.il.

‡ A.Z. and G.L. contributed equally to this work.

§ Ben Gurion University of the Negev.

|| University Medical Center.

⊥ University of Manchester.

The Hebrew University−Hadassah Medical School.

[1] Abbreviations: CD, circular dichroism; FN, fibronectin; HBS, heparin binding site; HSPG, heparan sulfate proteoglycans; IV, influenza virus; KIR, killer immunoglobulin-like receptors; LIR, leukocyte immunoglobulin-like receptors; MFI, mean fluorescence intensity; NCR, natural cytotoxicity receptor; NK, natural killer; PI, propidium iodide; RU, resonance units; SA, streptavidin.

10.1021/bi051241s CCC: $30.25
Published on Web 10/14/2005

cordance, tumor cells expressing cell surface heparanase, CHO cells lacking membranal heparan sulfate, and glypican-1-suppressed pancreatic cancer cells manifest reduced recognition by NKp46D2 and are lysed to a lesser extent by NK cells (*12*). The recognition and lysis of tumor cells by NK are also affected by the 6-O-sulfation and N-acetylation state of the glucosamine building unit of heparan sulfate (*12*).

Heparin and heparan sulfate bind to numerous proteins. The structural diversity of heparin and heparan sulfates is extremely vast, and the heparan sulfate moieties of cell membrane HSPGs modulate the binding and actions of a large number of extracellular and cellular molecules (*13*, *14*). In accordance, tumoral HSPGs might present infrequent or distinct heparan sulfate epitopes that contribute to tumor cell proliferation and cancer's angiogenesis (*15*−*17*); NKp46 could have evolved to recognize these epitopes and activate lysis of tumor cells by NK. Hence, in the current study we aimed to characterize the NKp46 heparan sulfate binding site and partially depict the epitope(s) it recognizes.

MATERIALS AND METHODS

Cells and Viruses. HeLa is a human cervical adenocarcinoma (ATCC no. CCL-2). 1106 is a human melanoma cell line established from a recurrent metastatic lesion and which expresses no HLA-I antigens (*18*). 293 is a human epithelial kidney cell line transformed with adenovirus 5 DNA (ATCC no. CRL-1573). Vero is an African green monkey fibroblast-like kidney cell line (ATCC no. CCL-81). The IV A/PR/8/34 (H1N1) was purchased from Spafas (Preston City, CT).

Ig Fusion Proteins. The generation of NKp46D2-Ig fusion protein was previously described (*7*, *12*). To generate NKp46D2/Q4-Ig, a set of external primers (Kozak-MGMP-fwd, TGAAAGCTTGCCGCCACCATGGGAATGCCCA-TGGGGTCTCTGCASACCG, and 44/46-endseq, GCCGTC-CACGTACCAGTTGAA) were used together with internal complementary primers (NKp46-Q4rev, CTGCTGTAC-CTGGCTGGATTGTCCCTCCTGGAGC, and NKp46-Q4fw, CAGGAGGGACAATCCAGCCAGGTACAGCAGGGA-TACG) synthesized with point mutations to create two PCR fragments (Q4L and Q4R). These fragments were mixed, denatured, and used again, as a template with the same external primers, to create one long fragment containing four point mutations: K133Q, R136Q, H139Q, and R142Q (designated D2/Q4). This D2/Q4 gene, fused to part of the human IgG1 Fc (CH2+CH3) gene (*12*), was then digested with *Kpn*I and *Bam*HI and inserted into pCDNA3.1-Fc, similarly digested, to create pCDNA3.1-D2/Q4-Fc. The same external primers were used together with a different set of internal complementary primers (NKp46 Q5rev, CTGTC-CCGTATCCCTGCTGTACCTGGCTGGATTGTCCCTCCT-GGAGC, and NKp46 Q5fw, CAGGAGGGACAATCCAGC-CAGGTACAGCAGGGATACGGGACAGTCCAG) to create, using the same techniques, the D2 fragment with five point mutations: K133Q, R136Q, H139Q, R142Q, and K146T in D2 (designated D2/Q4T1). This fragment was inserted, as described for the D2/Q4 fragment, into pCDNA3.1-Fc to create pCDNA3.1-Q4T1-Fc. 293 cells were transfected with these expression vectors, and G418-selected clones were screened for highest protein production. Recloned high-producer clones were grown in BIO-CHO-1 medium (Biological Industries, Kibbutz Beit Haemek, Israel), and supernatants were collected daily and purified on protein G columns using FPLC. SDS−PAGE analysis revealed that all Ig fusion proteins were approximately 95% pure and of the proper molecular mass.

Circular Dichroism (CD) Analysis. NKp46D2, NKp46D2/Q4, and NKp46D2/Q4T1 fusion proteins were analyzed for CD spectra at various concentrations: 0.66, 0.6, 0.48, 0.32, and 0.21 mg/mL in 300 μL of PBS. CD analysis was done on a J-715 CD spectral instrument with a bandwidth of 1 nm, response time of 1 s, data pitch of 0.2 nm, standard sensitivity, and scanning speed of 20 nm/min, at room temperature, and at the range of 250−200 nm using a 1 mm path length cuvette. Each sample was measured four times, and the average CD spectra were calculated automatically.

Flow Cytometry and Antibodies. Cells were incubated with the indicated micrograms of the various fusion Igs for 2 h at 4 °C, washed, and stained with FITC- or APC-conjugated $F(ab')_2$ goat anti-human IgG-Fcγ (109-096-098 or 109-136-098, respectively; Jackson ImmunoResearch, West Grove, PA). Staining and washing buffer consisted of 0.5% (w/v) BSA and 0.05% sodium azide in PBS. Propidium iodide (PI) was added prior to reading for exclusion of dead cells. Flow cytometry was performed using a FACSCalibur flow cytometer (Becton Dickinson, Mountain View, CA), and fluorescence data were acquired using logarithmic amplification. Data files were acquired and analyzed using BD CELLQuest 3.3 software. Fluorescence data were acquired using logarithmic amplification, and reported fluorescence intensity units represent conversion of channel values according to the logarithmic scale (range 10^0-10^4). Results are shown either as staining histograms (*X*-axis represents fluorescence intensity and *Y*-axis represents cell counts) or as the geometric mean fluorescence intensity (MFI) of the stained populations. In all experiments, each sample was stained twice in different wells. When results are presented as MFI, average MFI ± SD of the duplicate staining is brought to show consistency of the staining procedure. Human IgG1 (hIgG1 kappa, PHP010) was purchased from Serotec, Oxford, U.K.

Binding of Fusion Igs to IV-Infected Cells. 1106 melanoma cells (10^6/mL) were incubated overnight with 1000 units/mL IV. Cells (infected or uninfected) were washed and stained with NCR Igs as described above.

Direct Heparin Binding Assay. Plates were coated with 4 μg/mL amounts of various fusion proteins and hIgG1 (diluted with PBS, final volume 75 μL) overnight at 4 °C. Blocking buffer (150 μL/well of PBS supplemented with 0.05% Tween 20 and 2.5% dry skim milk) was applied for 2 h on ice, after which plates were washed with PBS with 0.05% Tween 20 (PBST) and incubated with 1 μg/mL biotin-tagged heparin (Sigma) for 1 h at 37 °C (100 μL/well). Following washing with PBST, 100 μL/well of streptavidin−HRP was added for 30 min at 1:2000 dilution in PBST supplemented with 0.5% skim milk. Following washing with PBST, 100 μL/well of TMB was added, and the color was allowed to develop at room temperature in the dark. Optical density was read at 650 nm (Dynex Technologies MRX microplate reader).

BIAcore. BIAcore 3000 (BIAcore AB, Uppsala, Sweden) was used for studying the interactions between heparin and NKp46D2. Heparin−albumin−biotin (Sigma) was immobilized on a streptavidin (SA) chip (BIAcore AB). The

immobilization process was performed with 10 mM Hepes buffer, pH = 7.4, 150 mM NaCl, and 0.005% Tween 20 (HBS buffer) at a flow rate of 10 μL/min. Heparin−albumin−biotin (20 μg/mL) was injected in 0.1 M sodium acetate buffer, pH = 4.5. The immobilization response was about 300 RU. Kinetic measurements: All experiments were performed at a flow rate of 20 μL/min in HBS buffer at 25 °C. Different analyte concentrations (from 0.125 to 2 or 4 μM) were injected, each followed by regeneration of the surface using 2 M NaCl with 20 mM NaOH. Data processing was done by BIAevaluation software 4.1 using the 1:1 langmuir binding model with mass transfer and baseline drift. An empty flow cell was used as a control and was subtracted from the responses obtained from the reaction surface. The χ^2 value is a standard statistical measure of the closeness to fit, representing the mean square of the signal noise. The results were plotted in sensorgrams and expressed in resonance units (RU) against time.

Heparin Oligomers and Selectively Desulfated Heparin Oligomers. Heparin and heparan sulfate were purchased from Sigma (H-3400n and H-9902, respectively). Heparin oligomers (6-, 8-, 10-, 12-, 14-, 16-mers) were described previously (*19*). Heparin 4-mers were kindly provided by Dr. Israel Vlodavsky (Technion, Israel). Different heparin disaccharides were also purchased from Sigma (H-1020, H-8892, H-9276, H-9142, H-9267, H-9392, H-1146, H-9401, H-9017). Selectively desulfated heparin oligomers were described previously (*20*). Briefly, heparin initially contained 97.7% of the *N*-sulfate groups, 89.3% of the 2-*O*-sulfate groups, and 92.4% of the 6-*O*-sulfate groups. De-N-sulfated/N-acetylated heparin contained 90.5% of the 2-*O*-sulfate groups, 85.3% of the 6-*O*-sulfates, and a very low amount of remaining *N*-sulfate groups (2.4%). De-2-O-sulfated heparin contained 80.2% of the 6-*O*-sulfate groups, 91.4% of the *N*-sulfate groups, and a residual 2.2% of the 2-*O*-sulfates. De-6-O-sulfated heparin contained 98.2% of the *N*-sulfate groups, 54.7% of the 2-*O*-sulfate groups, and a residual 4.2% of the 6-*O*-sulfates.

RESULTS

Prediction of the Heparin/Heparan Sulfate Binding Site of NKp46. We examined the residues in NKp46 that may be involved in heparin/heparan sulfate binding. Heparin and to a less extent heparan sulfate are negatively charged biological macromolecules due to their high content of negatively charged sulfo and carboxyl groups. Therefore, it seems that a region with a high positive surface potential could be a candidate site for heparin/heparan sulfate binding. The electrostatic potential was calculated for the NKp46 structure (PDB code 1oll) using Delphi (*21*) and was presented on the surface using Grasp (*22*). Inspection of the electrostatic potential map revealed that basic residues laying on β strands C and C′, and the connecting loop (*23*) highly donate to a positive potential region of the membrane-proximal domain of NKp46 (D2 domain). Similarly, electrostatic map analysis of NKp46 (*24*), based on the other crystal structure of NKp46 [PDB code 1P6F (*24*)], revealed a similar positive patch. This region includes the basic residues Lys 133 (157), Arg 136 (160), His 139 (163), and Arg 142 (166) (Figure 1). Please note that amino acid (aa) numbers are designated according to the NKp46 ectodomain [PDB code 1oll (*23*)] and aa numbers in parentheses are according to the NKp46 complete sequence (human NKp46 mRNA, AJ001383). Through the rest of the text we will apply the aa numbering according to PDB code 1oll. Lys 133, Arg 136, and His 139 highly contribute to the large positive patch seen in NKp46D2 (Figure 1). These results are compatible with the fact that only NKp46D2 is essential for binding to tumor cells and to heparin/heparan sulfate (*7*, *12*).

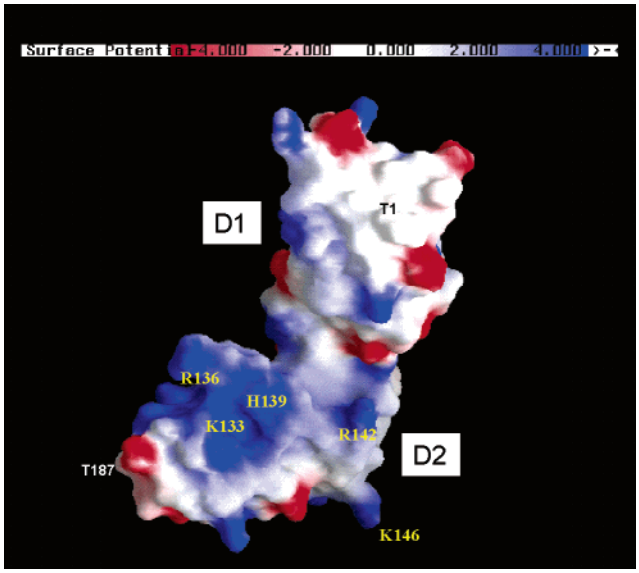

FIGURE 1: Electrostatic potential surface of NKp46 (PDB code 1oll). The potential map was calculated and depicted using the programs Delphi and Grasp (*21*, *22*). Delphi calculations of the electrostatic potential were performed using the full charges (prot_full) parameter set of Delphi. The surface is colored such that red is for negative potential (−4*kt*/e) and blue for positive potential (+4*kt*/e) changing gradually through white. The positive patch can be seen clearly at the NKp46D2 domain of the map. The location of the N-terminus and the C-terminus is shown by labeling Thr 1 and Thr 187. Amino acid labels are according to aa numbering of the NKp46 ectodomain (*23*). The corresponding aa numbers according to the NKp46 complete sequence (human NKp46 mRNA, AJ001383) are K157, R160, H163, R166, and K170 and (T25, T211) for the N- and C-termini of the ectodomain.

The assumption that this patch may be involved in heparin/heparan sulfate binding was further supported by another direction. The high folding similarity of NKp46 and the KIR2D NK receptors was already demonstrated (*23*). Indeed, running the sequence of NKp46 on the 3DPSSM threading server (*25*) revealed a significant sequence identity of NKp46 to that of a human KIR2D receptor (P58-C152 KIR, PDB code 1nkr). This protein appears as a member of the fibronectin type III superfamily. Further investigation of other members in this superfamily revealed a structure of human fibronectin (FN) type III repeats 12-14 that contains two heparin binding sites (PDB code 1fnh). The first is a primary one (HBS-1) located in FN13, and the second is a putative secondary binding site (HBS-2) which is ∼60 Å away in FN14 (*26*). HBS-1 appears in the structure as a continuous positively charged patch. The involvement of its residues in heparin binding was demonstrated by biochemical and mutagenesis data (*27*−*29*) and was further supported by the fact that these residues are conserved in FNs from frog to man (*30*−*32*). The existence of a secondary heparin binding site (HBS-2) was suggested since biochemical data indicate that both FN13 and FN14 are essential for full heparin binding (*27*, *28*). Synthetic peptides that contain part of

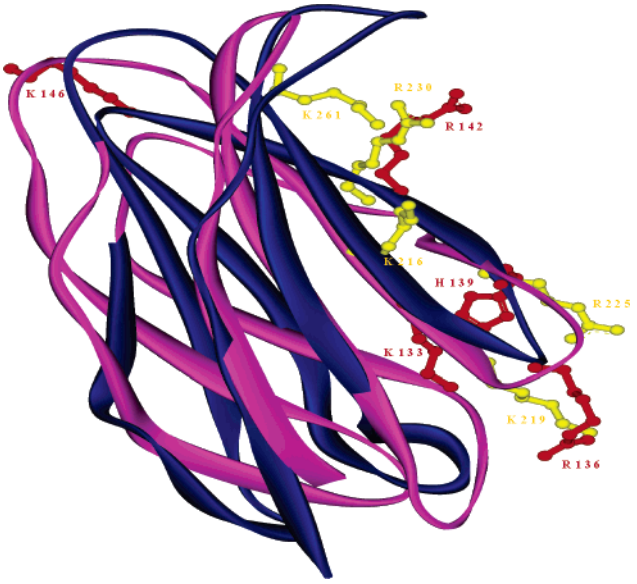

FIGURE 2: Superimposition of the FN14 and D2 domain of NKp46. Both proteins are depicted in a solid ribbon presentation, colored in magenta and blue for FN14 and NKp46, respectively. Side chains of basic residues associated with HBS-2 in FN14 and the positively charged region in NKp46 are depicted in ball and stick and colored in yellow and red, respectively. The residue labels correspond to the color of the side chains.

HBS-2 residues show heparin binding ability (*33*−*36*). In the crystal structure of FN12-14 HBS-2 appears as a positively charged region. This putative heparin binding site consists of a cluster of basic residues: Lys 216, Lys 219, Arg 225, Arg 230, and Lys 261. Superimposition of NKp46D2 with FN13 structures shows no spatial overlap between HBS-1 and the residues that generate the region with the positive potential in NKp46. However, superimposition of NKp46D2 with FN14 reveals a nice spatial fit of these two areas (Figure 2). Besides the general structural resemblance of these two regions (3.6 Å rmsd for Cα of residues 212−233 and 129−145 of FN14 and NKp46, respectively) the side chains of Arg 136, His 139, and Arg 142 of NKp46 lay very close to the side chains of Lys 219, Arg 225, and Arg 230 of FN14, respectively (Figure 2). On the basis of these observations it was suggested to mutate Lys 133, Arg 136, His 139, Arg 142, and Lys 146 into noncharged amino acids and to examine the binding of these mutants to heparin/heparan sulfate as compared to the wild type. Lys 146, the second residue that follows the C′ strand (*23*), was chosen due to its vicinity to Arg 142, which lay very close to Arg 230 in HBS-2 of fibronectin (FN) type III, as described above. The electrostatic map also indicates a possible role for Lys 146 together with Arg 142 in heparan sulfate epitope binding (Figure 1).

Construction of NKp46D2 Mutants and Binding to Tumor and Virus-Infected Cells. We used PCR with mutated oligonucleotides to construct Q4 (K133Q, R136Q, H139Q, and R142Q; four point mutations to hydrophilic, noncharged, amino acids) and Q4T1 (K133Q, R136Q, H139Q, R142Q, and K146T, five point mutations; aa numbers are according to PDB code 1oll). Corresponding fusion proteins were prepared (NKp46D2/Q4-Ig and NKp46D2/Q4T1-Ig) and compared to NKp46D2-Ig. Amino acid sequences of NKp46D2, NKp46D2/Q4-Ig, and NKp46D2/Q4T1-Ig at the putative heparan sulfate binding site are depicted in Figure 3A. Mutations did not affect the integrity of the different fusion Igs as revealed by SDS−PAGE analysis. To refute the possibility that the secondary structure of NKp46D2/Q4-Ig and NKp46D2/Q4T1-Ig was transformed as a result of the mutations, a circular dichroism (CD) analysis was applied; the proteins were diluted in PBS to various concentrations and analyzed for CD spectra. Comparing the spectra of the NKp46D2, NKp46D2/Q4-Ig, and NKp46D2/Q4T1-Ig fusion proteins showed a similar CD pattern indicating identical secondary structures (Figure 3B). The fluctuations at 200−205 nm are probably due to the high voltage (350 V and more) used at this point by the instrument at the edge of its measurement ability and can be ignored. Thus, it is likely to assume that the mutations in the putative heparin binding site did not alter the folding of the fusion proteins.

We next analyzed the binding of 293-produced NKp46D2-Ig, NKp46D2/Q4-Ig, and NKp46D2/Q4T1-Ig to influenza virus- (IV-) infected and uninfected 1106 melanoma cells (Figure 4A,B). We previously published that the NKp46 receptor recognized the HA of IV and that this binding is required for lysis of IV-infected cells (*6*, *8*, *9*). We further showed this IV−HA recognition was restricted to NKp46D2 (*7*). Thus, for tumor 1106 cells infected with the IV, both the membranal tumoral ligands and the IV−HA expressed on the membrane of infected cells contribute to the binding of NKp46D2. Binding of NKp46D2/Q4-Ig and NKp46D2/Q4T1-Ig to tumor cells was significantly reduced (2-fold and 5-fold, respectively) as compared to NKp46D2-Ig. However, enhancement of binding due to IV infection of 1106 cells was similar for NKp46D2 and its mutations, NKp46D2-Q4 and NKp46D2-Q4T1 (Figure 4A,B). Therefore, mutations in the putative heparin/heparan binding site significantly reduced binding to the tumoral ligands but not to the viral HA ligand.

We previously published that binding of NKp46D2-Ig to tumor cells is inhibited by heparin/heparan sulfate (*11*). We examined the ability of heparan sulfate to inhibit binding of the fusion Igs to tumor cells. The addition of heparan sulfate did not affect the binding of NKp46D2/Q4-Ig but reduced the binding of NKp46D2-Ig to a comparable level (Figure 4C). Therefore, suppression of tumor recognition, by blocking NKp46D2 binding with soluble heparan sulfate, equaled the effect of mutating the putative NKp46D2-heparan sulfate binding site on tumor binding.

Direct Binding of NKp46D2 and Mutants to Heparin/Heparan Sulfate. To determine more specifically the mutation effect on NKp46 interaction with heparin/heparan sulfate, we measured binding of the fusion proteins to their purified putative ligands on a solid matrix rather than on the cell surface. We compared the binding of NKp46D2-Ig, NKp46D2/Q4-Ig, NKp46D2/Q4T1-Ig, and hIgG1 to purified heparin in ELISA assays. Human IgG1 served as a negative control since the fusion Igs contained the Fc portion of hIgG1. For the assay, plates were coated with the different fusion Igs. The plates were then blocked, washed, and incubated with/without biotin-tagged heparin, followed by SA-HRP and TMB substrate for colorimetric detection. Without heparin, wells coated with all fusion Igs or hIgG1 manifested marginal background OD levels. When heparin was used in the assay, NKp46D2-Ig manifested heparin-specific binding while both mutations showed reduced

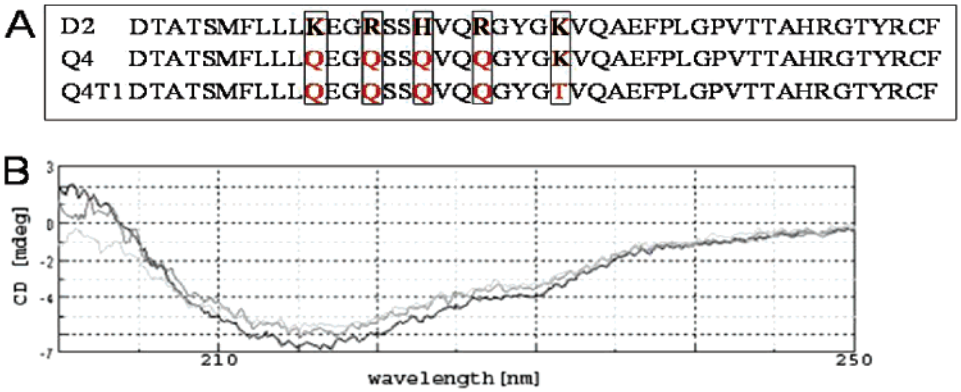

FIGURE 3: Amino acid sequence and CD spectra of NKp46D2 and mutations. (A) Amino acid sequence of NKp46D2, NKp46D2/Q4, and NKp46D2/Q4T1 at the putative heparan sulfate binding site. Amino acids depicted are from 123 to 167, according to the NKp46 ectodomain aa numbering (*23*). (B) CD curves shown are for NKp46D2-Ig (black), NKp46D2/Q4-Ig (light gray), and NKp46D2/Q4T1-Ig (dark gray). Protein concentrations were 0.32 mg/mL (approximately 3.5 μM) for NKp46D2-Ig and NKp46D2/Q4-Ig and 0.21 mg/mL (approximately 2.3 μM) in PBS for NKp46D2/Q4T1-Ig. CD spectral analysis was performed in a J-715 with a bandwidth of 1 nm, response time of 1 s, data pitch of 0.2 nm, standard sensitivity, and scanning speed of 20 nm/min, at room temperature, at the range of 250−200 nm with a 1 mm cuvette. Results are from one representative experiment of two.

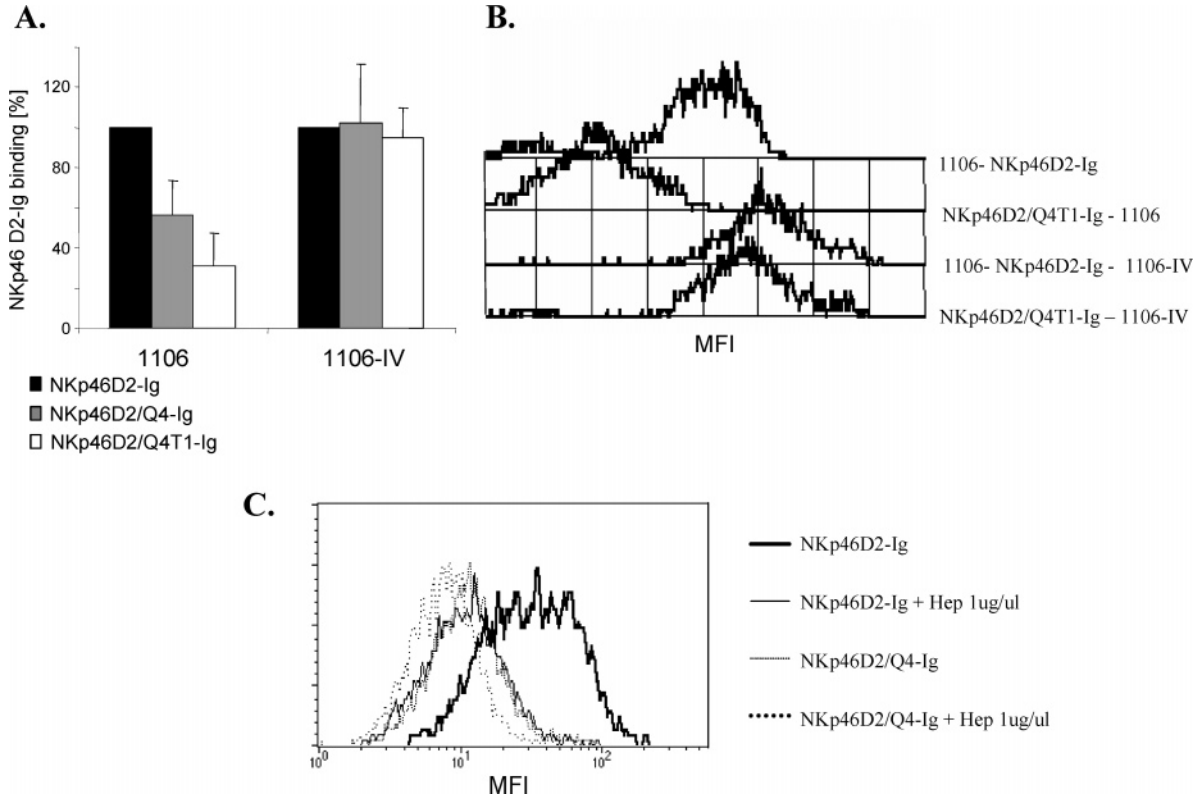

FIGURE 4: Binding of NKp46D2-Ig and NKp46D2 mutants to noninfected and IV-infected tumor cells and effect of heparan sulfate. (A, B) 1106 human melanoma cells (10^6/mL) were incubated overnight with/without 1000 units/mL IV. Cells (infected or uninfected) were washed, incubated with fusion Igs, and stained with FITC-anti-human Fc second antibody. (A) Comparison of NKp46D2 with NKp46D2/Q4 and NKp46D2/Q4T1 in which MFIs for duplicate staining with NKp46D2 were averaged and normalized to 100 and MFIs for staining with the mutant Igs were normalized accordingly. (B) Overlay of a representative experiment comparing NKp46D2 with NKp46D2/Q4T1. (C) Effect of heparan sulfate. Ten micrograms of NKp46D2-Ig or NKp46D2/Q4-Ig (in 100 μL final volume, 1.1 μM) was premixed with heparan sulfate (1 μg/mL, approximately 0.3 μM), and 10^5 Vero tumor cells were then added for 2 h at 4 °C, followed by staining with FITC-anti-Fc second antibody. Results are from one representative experiment of four (panels A and B) and two (panel C). PI was added to exclude dead cells. For panel A, MFI results are the average of two different samples assayed in the same experiment. Bars, ±SD (of the duplicate, indicating the consistency of the staining procedure).

heparin-specific binding, by 2-fold and more (Figure 5). As with binding to tumor cells (Figure 4), the Q4T1 mutation showed less binding to heparin as compared with the Q4 mutation.

Next, we studied the kinetics of NKp46D2/heparin binding using a BIAcore analysis system. Figure 6 shows a comparison of NKp46D2 and the two mutations. To estimate the affinity between heparin and NKp46D2 or NKp46D2 mutations, we injected increasing concentrations of the fusion Igs. Figure 6 shows overlays of sensorgrams resulting from the injection of increasing concentrations of NKp46D2-Ig (Figure 6A), NKp46D2/Q4-Ig (Figure 6B), and NKp46/Q4T1-Ig (Figure 6C) over immobilized heparin. The equilibrium dissociation constant (K_D) value for NKp46D2-Ig,

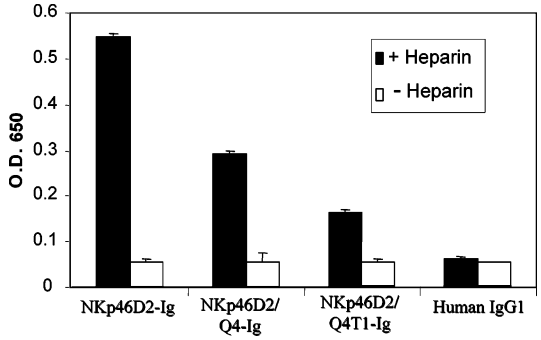

FIGURE 5: Direct binding of NKp46D2 and mutations to heparin. ELISA plates were coated with 4 μg/mL fusion Igs (44 nM) and hIgG1, followed by incubation with 1 μg/mL (0.66 μM) biotin-tagged heparin. Bound heparin was detected by SA-HRP. The data in the figure represent OD absorbance (650 nm). Results are from one representative experiment of three. Results are the average of four different samples assayed in the same experiment. Bars, ±SD.

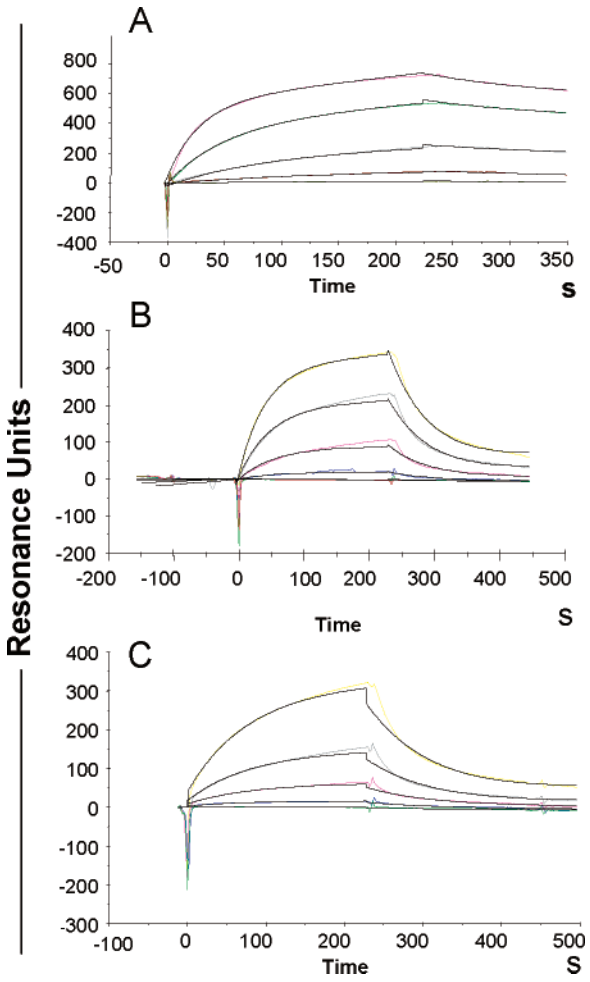

FIGURE 6: Kinetics of NKp46D2/heparin and mutated NKp46D2/heparin interactions. The results from the BIAcore analysis are expressed in resonance units (RU) against time. Dose-dependent binding of NKp46D2-Ig (A), NKp46D2/Q4-Ig (B), and NKp46D2/Q4T1-Ig (C) to heparin. Fusion Igs were injected over the heparin-immobilized surface at increasing concentrations ranging from 0 to 2 or 4 μM. Curves in all panels show specific binding after subtraction of background binding to the control flow cell (no heparin immobilized) and represent one of three experiments performed. The χ^2 values are 5.19, 6.9, and 4.61 for NKp46D2, NKp46D2/Q4, and NKp46D2/Q4T1, respectively.

NKp46D2/Q4-Ig, and NKp46/Q4T1-Ig was 0.41, 8.2, and 40.8 μM, respectively. NKp46D2-Ig displayed a binding

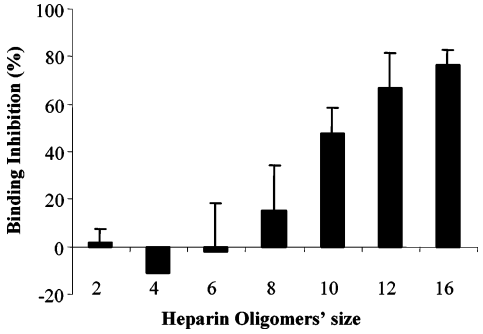

FIGURE 7: Effect of heparin oligomers on binding of NKp46D2-Ig to tumor cells. Ten micrograms of NKp46D2-Ig (in 100 μL final volume, 1.1 μM) was premixed with different size heparin oligomers (5 μg/mL), and 10^5 tumor cells were then added for 2 h at 4 °C. After incubation, tumor cells were washed and incubated with FITC-anti-Fc second antibody. PI was added to exclude dead cells. Results are presented as the percentage of inhibition of NKp46D2-Ig staining without premix with oligomers. Results are the summary of two independent experiments with a total of four different samples per point. A heparin disaccharide mix of H-9401 and H-9017 (Sigma) was used in these specific experiments. Other disaccharides (see Materials and Methods), tested in other experiments, did not inhibit either. Bars, ±SD.

curve to heparin with a K_{on} rate of 7.23 × 103 (M s)$^{-1}$ and a K_{off} rate of 2.96 × 10^{-3} s^{-1}. The K_{off} rate of the mutated fusion Igs was more than 10-fold higher, 1.64 × 10^{-2} and 1.21 × 10^{-2} for Q4 and Q4T1, respectively. These differences account mostly for the 1-log- and 2-log-fold higher K_D of Q4 and Q4T1. Again, the Q4T1 mutation manifested reduced binding to heparin as compared to the Q4 mutation, emphasizing the significance of K146 in the NKp46D2 heparin/heparan sulfate binding site. The K_D calculated for the heparin/heparan sulfate binding site in NKp46D2 is well in the midst of the range of K_Ds reported for heparin/heparan sulfate binding sites of other proteins (e.g., 39 nM for FGF2, 4 μM for the major binding site of tenacin-C, 2 μM for endostatin, and 3.2 μM for FGFR1) (*20*, *37*, *38*).

Partial Characterization of the Heparan Sulfate Epitope(s) Recognized by NKp46. Heparan sulfate manifests a high degree of structural diversity and contains a large number of defined specific epitopes that do not occur randomly and are tightly and topologically regulated (*14*, *39*). We first tested the minimal length of heparin oligomers that could inhibit binding of NKp46D2 to tumor cells. We tested 2−16-mers of heparin. The 2-, 4-, and 6-mers did not inhibit NKp46D2-Ig binding. The 4-mer even partly enhanced binding but at higher concentrations showed no effect (data not shown). The 8-mers manifested small inhibition while the 10−16-mers showed increased inhibition in correlation with the size of the heparin oligomers (Figure 7).

To partially characterize the sulfate groups of heparin/heparan sulfate involved in the recognition by NKp46D2, we tested the ability of selectively desulfated heparin oligomers to inhibit binding of NKp46D2 to (i) HeLa tumor cells as measured by flow cytometry (Figure 8A) and (ii) immobilized heparin as measured by BIAcore (Figure 8B). The inhibition ability of these selectively desulfated heparin oligomers was compared to that of LMW heparin and heparan sulfate. In this experimental setup, a strong inhibition of a particular desulfated heparin oligomer indicated that the removed sulfate groups were not involved in the heparin/heparan sulfate interaction and vice versa. HeLa cells were

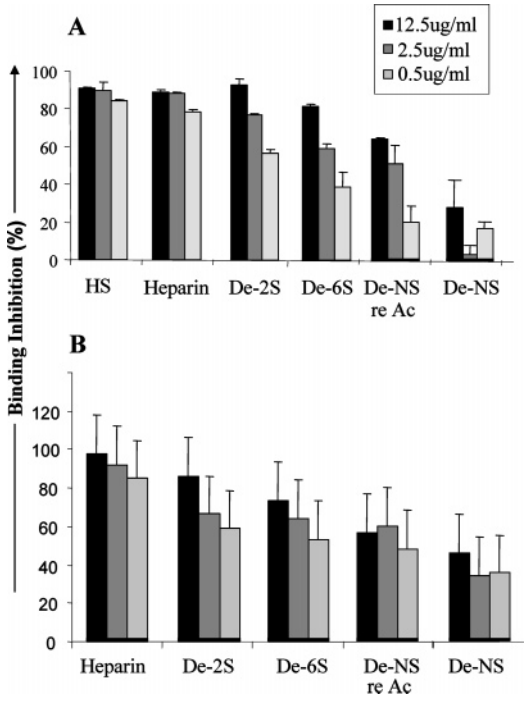

FIGURE 8: Effect of selectively monodesulfated heparin oligomers on binding of NKp46D2-Ig to tumor cells and to immobilized heparin. (A) Ten micrograms of NKp46D2-Ig (in 100 μL final volume, 1.1 μM) was premixed with different monodesulfated heparin oligomers (12.5, 2.5, and 0.5 μg/mL), and 10^5 tumor cells were then added for 2 h at 4 °C. After incubation, tumor cells were washed and incubated with APC-anti-Fc second antibody. PI was added to exclude dead cells. Results are presented as the percentage of inhibition of NKp46D2-Ig staining without premix with oligomers. Results are the summary of two independent experiments with a total of four different samples per point. Bars, ±SD. (B) A BIAcore streptavidin (SA) chip was immobilized with biotin-tagged heparin (50 RU). NKp46D2-Ig (1 μM) was preincubated with 12.5, 2.5, and 0.5 μg/mL selectively monodesulfated heparin oligomers for 1 h at room temperature prior to injection over immobilized heparin. Results are presented as the percentage of inhibition of NKp46D2-Ig binding to immobilized heparin without premix with oligomers. Results are representative of two independent experiments. Bars, ±SD.

incubated with selectively desulfated oligomers and NKp46D2-Ig; results shown in Figure 8A indicate that N-sulfation effectively contributed to the interaction of NKp46D2 with tumor cells. The contribution of 6-O-sulfation was also considerable, while the contribution of 2-O-sulfation was less significant. The improvement in inhibitory activity with N-acetylation of N-desulfated oligomers may reflect a contribution of the *N*-acetyl group to membranal heparan sulfate-mediated tumor recognition by NKp46D2. For assessment of direct binding of NKp46D2 to heparin, desulfated heparin oligomers were incubated for 1 h with NKp46D2-Ig before injection over immobilized heparin (Figure 8B). Again, if a particular desulfated heparin retained its ability to interact with NKp46D2, the injection of the complex resulted in inhibition of NKp46D2 binding to immobilized heparin. Results from oligomers' effects on direct binding studies were compatible with the results obtained for binding to tumor cells.

DISCUSSION

We previously published that tumoral HSPGs are recognized by NKp46 and that recognition of heparan sulfate moieties of the HSPGs is imperative for lysis of tumor cells by NK cells (*12*). In this study we aimed to identify the heparan sulfate binding site of NKp46. We predicted that a region in NKp46 with a high positive surface potential could be a candidate site for heparan sulfate binding. An electrostatic potential map was calculated for the NKp46 protein structure (PDB code 1oll). Its inspection revealed that basic residues located on β strands C and C′ and the connecting loop compiled a positive potential region on the NKp46D2 domain (Figure 1). In addition, superimposition of NKp46D2 with human fibronectin FN14 revealed a nice spatial fit of this NKp46D2-positive potential region and the heparin binding site 2 of FN14 (Figure 2). The NKp46D2 linearly contiguous sequence in β strands C and C′, predicted to be involved in heparin/heparan sulfate binding, did not contain consensus sequences for the β strand-based HBS site (e.g., XBBXBX, where B is a basic aa and X is a hydropathic aa) (13). Rather, it was similar to the structural motif suggested by Margalit and co-workers in which a distance of approximately 20 Å between two basic amino acids, facing opposite directions of an α helix or a β strand, is important for interaction with heparin (*40*). Other basic residues between these two basic amino acids at the extremes of the motif were suggested to face the same side of the secondary structure that binds heparin. A distance of 20 Å fits an accommodation of a pentasaccharide. The distance between R136 Cα and R142 Cα, in the structure of NKp46D2, which turn to opposite sides is 19 Å. K133 and H139, emerging from two different β strands, spatially stand between R136 and R142 and face the same side.

Mutating the positively charged K133, R136, H139, R142, and K146 aa of NKp46D2 into a noncharged amino acid suppressed the ability of these mutants to bind tumor cells as compared with the wild-type NKp46D2. Yet, no effect was observed on binding of NKp46 to viral ligands, indicating the specificity of these residues to the tumor binding site (Figure 4A,B). The reduced binding of the NKp46D2 mutants to tumor cells correlated with their reduced binding and affinity to heparin/heparan sulfate as measured by ELISA and BIAcore (Figures 5 and 6). Mutating four amino acids at once (NKp46D2/Q4-Ig) made it difficult to point out which aa is most important for binding heparin, but comparing it to the five aa mutant (NKp46D2/Q4T1-Ig) indicated a significant role for the fifth mutation. Indeed, the K146 mutation intensified the reduction in binding to both tumor cells and to purified heparin/heparan sulfate (Figures 4−6). Yet, mutating K146 (Lys) to Thr instead of Gln might instigate a greater effect; replacing the long positively charged residue with a much shorter uncharged residue (with no NH_2 group) resulted in changing charge, content, and distance between the side chain and the heparin/heparan sulfate. The importance of K146, which lay four residues away from R142 along the β strand of NKp46D2, to heparin binding suggests a binding of a heparin molecule longer than a pentasaccharide. The distance between the Cαs of R136 and K146 is 31 Å. This distance fits an accommodation of an octasaccharide which is about 30 Å in length. This prediction is in agreement with the experimental results that heparin oligomers with ≥eight ring length inhibit the binding of NKp46D2 to tumor cells, while those with two, four, and six do not exhibit any inhibition effect (Figure 7). The requirement for an extended heparin

```
          133   136   139   142                 146
NKp46     K E G R S S H V Q R G Y - - - - - - G K
LIR1      K E g E d e h p Q C L N s q p h a r g S
LIR2      K e g e d e h p Q C I n s q p h a r g s
KIR2DL1   R E g e - a h e R R L P a g p k v n g t
KIR2DL2   R E g e - a h E C R F S a g p k v n g t
KIR2DL3   R E g e - a h E R R F S a g p k v n g t
```

FIGURE 9: Alignment of NKp46D2, LIR, and KIR sequences. NKp46D2 sequences at the putative heparan sulfate binding site are aligned to the corresponding sequences of receptors from the KIR and LIR group. Amino acid numbering is of the NKp46 ectodomain (PDB code 1oll), and alignment is based on data from Ponassi et al. (*23*).

sequence for binding to NKp46D2 is somewhat analogous to the HBS-2 domain of fibronectin which shares some structural similarity with the studied NKp46D2-positive potential region (Figure 2) and also accommodates a long sequence with optimum binding being achieved with saccharides of 14/16 sugars in length (*41*, *42*). It is known that heparin interacts most tightly with protein sequences containing a complementary binding site of high positive charge density, while less sulfated heparan sulfate interacts most tightly with a complementary site on a sequence that has more widely spaced basic residues (*43*). The mutated amino acids are somehow dispersed, but there was no difference in binding heparan sulfate or heparin as measured by their ability to inhibit binding of NKp46D2 to HeLa cells (Figure 8A).

Analysis of the PDB shows that tandem Ig-like domain arrangements comparable to NKp46 are present in leukocyte immunoglobulin-like receptors (LIRs) and killer immunoglobulin-like receptors (KIRs) (*23*). Therefore, it is interesting to compare the five positively charged residues of NKp46D2 studied here to residues in LIRs and KIRs at the corresponding positions, using the sequence alignment presented by Ponassi et al. (*23*) (Figure 9). The position of NKp46 K133 is positively charged in all six structures. However, R136 in NKp46 is replaced to negatively charged Glu in both LIR and KIRs. Furthermore, in the LIRs Ser 137 and Ser 138 of NKp46 are replaced by the negatively charged Asp and Glu, respectively. H139 in NKp46 is conserved in all six structures. R142 of NKp46 is conserved in the KIRs but replaced to Cys in the LIRs. K146 in NKp46 is either Ser or Thr in both LIRs and KIRs. The total charge of the whole investigated region (K133−K146, in NKp46) is clearly more positive in NKp46 than in the LIRs and the KIRs. The positively charged patch that appears in NKp46 in this region disappears in the calculated potential map of the LIRs (data not shown). Overall, these comparisons suggest that the binding of LIRs and KIRs to heparin in this region will be much weaker, if any, compared to that of NKp46. In accordance, we showed that neither LIR1 nor KIR2DL1 and KIR2DL2 binding to tumor cells involves heparan sulfate proteoglycans (*12*).

The interaction of NKp46 with heparan sulfate epitope(s) on HSPGs can facilitate its binding to other, hitherto elusive, cellular ligands. For example, the heparan sulfate epitope(s) can serve as coligands, similar to heparin/heparan sulfate interaction with either growth factors and growth factor receptors or with lipid binding proteins (*13*, *44*). Recognition of stromal cells by CD19, a coreceptor of the B-cell receptor, was shown to involve HSPGs expressed by the stromal cells (*45*). Alternatively, tumor-modified heparan sulfate can overexpress certain existing epitope(s) or express separate unique carbohydrate epitope(s) recognized distinctively by NKp46 that are rarely expressed on membranal heparan sulfate of normal cells. We were able to partially characterize the heparan sulfate epitope(s) recognized by NKp46. We previously published that 6-O-sulfation and N-acetylation state of the glucosamine building unit affect NKp46-tumor recognition and lysis by NK cells (*12*). At the present study, we performed a more detailed analysis using selectively monodesulfated heparin oligomers and studying NKp46D2 binding to both tumor cells and immobilized heparin. The tumor-expressed heparan sulfate's epitope and the immobilized heparin's epitope recognized by NKp46D2 manifested a similar phenotype. N-Sulfation strongly contributed to the binding; 6-O-sulfation and N-acetylation had a moderate contribution while 2-O-sulfation manifested a smaller effect (Figure 8). We previously showed that complete O-desulfation of heparin significantly reduced its ability to inhibit NKp46D2 binding to tumor cells (*12*); thus, the contribution of 2-O- and 6-O-sulfation is essential for epitope recognition by NKp46.

The exact sequence(s) and the cross-reactivity of the epitope(s) recognized by NKp46 remain to be explored. Yet, it is clear that heparan sulfate exhibits a considerable number of unique overlapping sequences with peculiar sulfating profiles and these sequences are recognized by specific complementary proteins (*46*). If unusual heparan sulfate epitopes on cancer cell membranes lead to better signaling through growth factor receptors, it might be that NK-expressed NKp46 evolved to recognize and penalize the uncommon epitope-expressing transformed cells. If so, this recognition can be considered as "transformed cell pattern recognition" by NK cells, similar to pattern recognition of infectious agents employed by innate immunity in which NKs play a central role.

ACKNOWLEDGMENT

We thank Mrs. N. Gasiunas for the preparation of the heparin oligomers. We are grateful to Dr. Zer Hagit from the Hebrew University of Jerusalem for assistance in BIAcore studies.

REFERENCES

1. Trinchieri, G. (1989) Biology of natural killer cells, *Adv. Immunol. 47*, 187−376.
2. Long, E. O. (2002) Tumor cell recognition by natural killer cells, *Semin. Cancer Biol. 12*, 57−61.
3. Biassoni, R., Cantoni, C., Pende, D., Sivori, S., Parolini, S., Vitale, M., Bottino, C., and Moretta, A. (2001) Human natural killer cell receptors and co-receptors, *Immunol. Rev. 181*, 203−214.
4. Bakker, A. B., Wu, J., Phillips, J. H., and Lanier, L. L. (2000) NK cell activation: distinct stimulatory pathways counterbalancing inhibitory signals, *Hum. Immunol. 61*, 18−27.
5. Moretta, A., Bottino, C., Vitale, M., Pende, D., Cantoni, C., Mingari, M. C., Biassoni, R., and Moretta, L. (2001) Activating receptors and coreceptors involved in human natural killer cell-mediated cytolysis, *Annu. Rev. Immunol. 19*, 197−223.
6. Arnon, T. I., Lev, M., Katz, G., Chernobrov, Y., Porgador, A., and Mandelboim, O. (2001) Recognition of viral hemagglutinins by NKp44 but not by NKp30, *Eur. J. Immunol. 31*, 2680−2689.
7. Arnon, T. I., Achdout, H., Lieberman, N., Gazit, R., Gonen-Gross, T., Katz, G., Bar-Ilan, A., Bloushtain, N., Lev, M., Joseph, A., Kedar, E., Porgador, A., and Mandelboim, O. (2004) The mechanisms controlling the recognition of tumor and virus infected cells by NKp46, *Blood 103*, 664−672.

8. Mandelboim, O., Lieberman, N., Lev, M., Paul, L., Arnon, T. I., Bushkin, Y., Davis, D. M., Strominger, J. L., Yewdell, J. W., and Porgador, A. (2001) Recognition of haemagglutinins on virus-infected cells by NKp46 activates lysis by human NK cells, *Nature 409*, 1055−1060.
9. Mandelboim, O., and Porgador, A. (2001) NKp46, *Int. J. Biochem. Cell Biol. 33*, 1147−1150.
10. Arnon, T. I., Achdout, H., Levi, O., Markel, G., Saleh, N., Katz, G., Gazit, R., Gonen-Gross, T., Hanna, J., Nahari, E., Porgador, A., Honigman, A., Plachter, B., Mevorach, D., Wolf, D. G., and Mandelboim, O. (2005) Inhibition of the NKp30 activating receptor by pp65 of human cytomegalovirus, *Nat. Immunol. 6*, 515−523.
11. Porgador, A. (2005) Natural cytotoxicity receptors: pattern recognition and involvement of carbohydrates, *Sci. World J. 5*, 151−154.
12. Bloushtain, N., Qimron, U., Bar-Ilan, A., Hershkovitz, O., Gazit, R., Fima, E., Korc, M., Vlodavsky, I., Bovin, N. V., and Porgador, A. (2004) Membrane-associated heparan sulfate proteoglycans are involved in the recognition of cellular targets by NKp30 and NKp46, *J. Immunol. 173*, 2392−2401.
13. Capila, I., and Linhardt, R. J. (2002) Heparin-protein interactions, *Angew. Chem., Int. Ed. Engl. 41*, 391−412.
14. Sasisekharan, R., and Venkataraman, G. (2000) Heparin and heparan sulfate: biosynthesis, structure and function, *Curr. Opin. Chem. Biol. 4*, 626−631.
15. Kleeff, J., Ishiwata, T., Kumbasar, A., Friess, H., Buchler, M. W., Lander, A. D., and Korc, M. (1998) The cell-surface heparan sulfate proteoglycan glypican-1 regulates growth factor action in pancreatic carcinoma cells and is overexpressed in human pancreatic cancer, *J. Clin. Invest. 102*, 1662−1673.
16. Lai, J., Chien, J., Staub, J., Avula, R., Greene, E. L., Matthews, T. A., Smith, D. I., Kaufmann, S. H., Roberts, L. R., and Shridhar, V. (2003) Loss of HSulf-1 up-regulates heparin-binding growth factor signaling in cancer, *J. Biol. Chem. 278*, 23107−23117.
17. Matsuda, K., Maruyama, H., Guo, F., Kleeff, J., Itakura, J., Matsumoto, Y., Lander, A. D., and Korc, M. (2001) Glypican-1 is overexpressed in human breast cancer and modulates the mitogenic effects of multiple heparin-binding growth factors in breast cancer cells, *Cancer Res. 61*, 5562−5569.
18. Porgador, A., Mandelboim, O., Restifo, N. P., and Strominger, J. L. (1997) Natural killer cell lines kill autologous beta2-microglobulin-deficient melanoma cells: implications for cancer immunotherapy, *Proc. Natl. Acad. Sci. U.S.A. 94*, 13140−13145.
19. Goger, B., Halden, Y., Rek, A., Mosl, R., Pye, D., Gallagher, J., and Kungl, A. J. (2002) Different affinities of glycosaminoglycan oligosaccharides for monomeric and dimeric interleukin-8: a model for chemokine regulation at inflammatory sites, *Biochemistry 41*, 1640−1646.
20. Ricard-Blum, S., Feraud, O., Lortat-Jacob, H., Rencurosi, A., Fukai, N., Dkhissi, F., Vittet, D., Imberty, A., Olsen, B. R., and van der Rest, M. (2004) Characterization of endostatin binding to heparin and heparan sulfate by surface plasmon resonance and molecular modeling: role of divalent cations, *J. Biol. Chem. 279*, 2927−2936.
21. Nicholls, A., and Honig, B. (1991) Rapid finite difference algorithm, utilizing successive over-relaxation to solve the Poisson−Boltzmann equation, *J. Comput. Chem. 12*, 435−445.
22. Nicholls, A., Sharp, K. A., and Honig, B. (1991) Protein folding and association: insights from the interfacial and thermodynamic properties of hydrocarbons, *Proteins 11*, 281−296.
23. Ponassi, M., Cantoni, C., Biassoni, R., Conte, R., Spallarossa, A., Pesce, A., Moretta, A., Moretta, L., Bolognesi, M., and Bordo, D. (2003) Structure of the human NK cell triggering receptor NKp46 ectodomain, *Biochem. Biophys. Res. Commun. 309*, 317−323.
24. Foster, C. E., Colonna, M., and Sun, P. D. (2003) Crystal structure of the human natural killer (NK) cell activating receptor NKp46 reveals structural relationship to other leukocyte receptor complex immunoreceptors, *J. Biol. Chem. 278*, 46081−46086.
25. Kelley, L. A., MacCallum, R. M., and Sternberg, M. J. (2000) Enhanced genome annotation using structural profiles in the program 3D-PSSM, *J. Mol. Biol. 299*, 499−520.
26. Sharma, A., Askari, J. A., Humphries, M. J., Jones, E. Y., and Stuart, D. I. (1999) Crystal structure of a heparin- and integrin-binding segment of human fibronectin, *EMBO J. 18*, 1468−1479.
27. Ingham, K. C., Brew, S. A., and Atha, D. H. (1990) Interaction of heparin with fibronectin and isolated fibronectin domains, *Biochem. J. 272*, 605−611.
28. Barkalow, F. J., and Schwarzbauer, J. E. (1991) Localization of the major heparin-binding site in fibronectin, *J. Biol. Chem. 266*, 7812−7818.
29. Busby, T. F., Argraves, W. S., Brew, S. A., Pechik, I., Gilliland, G. L., and Ingham, K. C. (1995) Heparin binding by fibronectin module III-13 involves six discontinuous basic residues brought together to form a cationic cradle, *J. Biol. Chem. 270*, 18558−18562.
30. DeSimone, D. W., Spiegel, E., and Spiegel, M. (1985) The biochemical identification of fibronectin in the sea urchin embryo, *Biochem. Biophys. Res. Commun. 133*, 183−188.
31. Norton, P. A., and Hynes, R. O. (1987) Alternative splicing of chicken fibronectin in embryos and in normal and transformed cells, *Mol. Cell. Biol. 7*, 4297−4307.
32. Hynes, R. O., Schwarzbauer, J. E., and Tamkun, J. W. (1984) Fibronectin: a versatile gene for a versatile protein, *Ciba Found. Symp. 108*, 75−92.
33. McCarthy, J. B., Chelberg, M. K., Mickelson, D. J., and Furcht, L. T. (1988) Localization and chemical synthesis of fibronectin peptides with melanoma adhesion and heparin binding activities, *Biochemistry 27*, 1380−1388.
34. McCarthy, J. B., Skubitz, A. P., Qi, Z., Yi, X. Y., Mickelson, D. J., Klein, D. J., and Furcht, L. T. (1990) RGD-independent cell adhesion to the carboxy-terminal heparin-binding fragment of fibronectin involves heparin-dependent and -independent activities, *J. Cell Biol. 110*, 777−787.
35. Drake, S. L., Varnum, J., Mayo, K. H., Letourneau, P. C., Furcht, L. T., and McCarthy, J. B. (1993) Structural features of fibronectin synthetic peptide FN−C/H II, responsible for cell adhesion, neurite extension, and heparan sulfate binding, *J. Biol. Chem. 268*, 15859−15867.
36. Woods, A., McCarthy, J. B., Furcht, L. T., and Couchman, J. R. (1993) A synthetic peptide from the COOH-terminal heparin-binding domain of fibronectin promotes focal adhesion formation, *Mol. Biol. Cell 4*, 605−613.
37. Ibrahimi, O. A., Zhang, F., Hrstka, S. C., Mohammadi, M., and Linhardt, R. J. (2004) Kinetic model for FGF, FGFR, and proteoglycan signal transduction complex assembly, *Biochemistry 43*, 4724−4730.
38. Jang, J. H., Hwang, J. H., Chung, C. P., and Choung, P. H. (2004) Identification and kinetics analysis of a novel heparin-binding site (KEDK) in human tenascin-C, *J. Biol. Chem. 279*, 25562−25566.
39. Dennissen, M. A., Jenniskens, G. J., Pieffers, M., Versteeg, E. M., Petitou, M., Veerkamp, J. H., and van Kuppevelt, T. H. (2002) Large, tissue-regulated domain diversity of heparan sulfates demonstrated by phage display antibodies, *J. Biol. Chem. 277*, 10982−10986.
40. Margalit, H., Fischer, N., and Ben-Sasson, S. A. (1993) Comparative analysis of structurally defined heparin binding sequences reveals a distinct spatial distribution of basic residues, *J. Biol. Chem. 268*, 19228−19231.
41. Walker, A., and Gallagher, J. T. (1996) Structural domains of heparan sulphate for specific recognition of the C-terminal heparin-binding domain of human plasma fibronectin (HEPII), *Biochem. J. 317*, 871−877.
42. Lyon, M., Rushton, G., Askari, J. A., Humphries, M. J., and Gallagher, J. T. (2000) Elucidation of the structural features of heparan sulfate important for interaction with the Hep-2 domain of fibronectin, *J. Biol. Chem. 275*, 4599−4606.
43. Fromm, J. R., Hileman, R. E., Caldwell, E. E., Weiler, J. M., and Linhardt, R. J. (1997) Pattern and spacing of basic amino acids in heparin binding sites, *Arch. Biochem. Biophys. 343*, 92−100.
44. Ornitz, D. M., and Itoh, N. (2001) Fibroblast growth factors, *Genome Biol. 2*, 1−12.
45. de Fougerolles, A. R., Batista, F., Johnsson, E., and Fearon, D. T. (2001) IgM and stromal cell-associated heparan sulfate/heparin as complement-independent ligands for CD19, *Eur. J. Immunol. 31*, 2189−2199.
46. Sugahara, K., and Kitagawa, H. (2002) Heparin and heparan sulfate biosynthesis, *IUBMB Life 54*, 163−175.

BI051241S